Spline-Galerkin methods applied to Rydberg series between the $4s\ ^2S$ and $3d\ ^2D$ limits of calcium

Tomas Brage
Code 681, National Research Council, Goddard Space Flight Center, Greenbelt, Maryland 20771

Charlotte Froese Fischer
Vanderbilt University, Box 1679B, Nashville, Tennessee 37235

(Received 6 December 1993; revised manuscript received 28 April 1994)

The recently introduced nonvariational spline-Galerkin method [T. Brage and C. Froese Fischer, Phys. Scr. **49**, 651 (1994)] for Rydberg series is applied to the $J=0$, 1, 2, and 3 even states between the two first limits in neutral calcium. Energies for $3dnl$ levels up to $n=15$–20 are reported and the position of different perturbers belonging to the $4p^2$ and $4p5p$ configurations are investigated. The $4p5p\ ^1P_1$ level is predicted to have an excitation energy of about 61 200 cm^{-1} and the $4p5p\ ^3D$ level is predicted at about 61 600–62 000 cm^{-1}, while the $4p5p\ ^3P$ is just at the $3d\ ^2D$ limit.

PACS number(s): 31.20.Tz, 32.80.Rm

I. INTRODUCTION

The study of Rydberg series presents us with many fascinating challenges. In some cases a number of series are interleaved and interact strongly. The presence of perturbers causes irregularities and gives important contributions to the observed spectra. The identification and labeling of these perturbers has caused a lot of activity in recent years, where different methods give quite different answers (see [1] and references therein).

Calcium is of particular interest due to its special complications originating in the fact that the outermost core subshell is $3p^6$, while the $3d$ subshell is empty. Even though the $4s$ electron has the largest binding energy, the $3d$'s binding energy is similar to both that of $4s$ and $4p$ shells. Therefore there are many overlaps between series with different limits, causing strong perturbations. An added complication is the strong correlation between the $3d$ subshell and, primarily, the $3p$ core subshell. To use a very simplistic argument, the fact that these two subshells have the same n quantum number gives important contributions from core-valence correlation. Calculations that include this differ in essential ways from ones which only treat the valence correlation [2,3].

Earlier works have mainly been concerned with the truly bound Rydberg series of calcium, below the first ionization limit $4s\ ^2S$ [4]. In this work we will concentrate on the interesting, and in many ways more complex, region, between this limit and the second one, $3d\ ^2D$. Here a number of Rydberg series, of the form $3dnl$, are interleaved and perturbers exist in the whole range, from among the first few members of the series to close to the $3d$ limit. The only other calculations for the even series [5] reported on these systems utilize the eigenchannel R-matrix method and multichannel quantum-defect theory [6–8]. On the experimental side, for the even-parity states, the only investigation concerns the $J=0$ and 2 states [9]. The odd series, of the form $3dnp$ and $3dnf$, have been studied much more extensively both experimentally [10–12] and theoretically [12–16].

In this paper we use the recently introduced [16,17] spline-Galerkin method to investigate these $3dnl$ series. We are interested in both a nonrelativistic treatment, to detect the possible perturbers (the $4pnp$ perturbers are quite well described in LS coupling), and a relativistic approach, where shifts and spin-dependent effects are included in the form of Breit-Pauli operators. The earlier works are concerned only with $J=0$ and 2, while here we extend the study to include also $J=1$ and 3.

II. THEORETICAL METHOD

The approach used in this work basically consists of two different steps: first the spline-Galerkin method, which leads to a generalized eigenvalue problem, and second the Breit-Pauli configuration-interaction (CI) calculation, where the relativistic effects are added. The method has recently been described in quite some detail, both for continuum- [17] and bound-state calculations [16], so we will only outline here the most important properties and assumptions of the method.

Very important for the present discussion is the multichannel form of the atomic state function (ASF) with pseudostates. In the nonrelativistic case it is

$$\Psi(\gamma LS)=\sum_{i=1}^{M_p} c(i)\phi(\alpha_i LS)+\sum_{i=1}^{M_c}\overline{\Phi}(\gamma_i LS)\ . \tag{1}$$

We use a notation where all functions that are overlined are unnormalized. The first sum in this equation is over configuration state functions (CSFs), which consist of a coefficient times a fixed, normalized pseudo-CSF. The second includes channel CSFs

$$\overline{\Phi}(\gamma_i LS)=|(\text{target}_i\cdot|\overline{n_i l_i}\rangle)^{(2S+1)}L\rangle\ . \tag{2}$$

The $|\overline{n_i l_i}\rangle$ denotes an unrenormalized channel function

$$|\overline{n_i l_i}\rangle=\overline{P}_{n_i l_i}|l_i s\rangle\ , \tag{3}$$

where $|l_i s\rangle$ denotes the spin angular part of the one-electron function. In the calcium case, the target is a

CSF with one electron outside the closed core. The notation implies that the channel function is coupled to the target according to the usual angular momentum rules, to form a total L and S. The basic philosophy will now be that all the radial functions for the target and the pseudostates are taken from Hartree-Fock calculations for Ca^+. For a given set of limits, all possible pseudostates, with two electrons outside the closed core, and all possible channels, which can couple to the given LS, are included. To be able to treat the quasibound states above the $4s\ ^2S$ limit we exclude all pseudostates and channels built on this limit and orthogonalize all s channel functions to the Hartree-Fock $4s$ level of Ca^+.

As an example, let us look at the $^1D^e$ series. We include the target states

$$3d\ ^2D,\ 4p\ ^2P,\ 5s\ ^2P,\ 4d\ ^2D,\ 5p\ ^2P,\ 4f\ ^2F\ , \tag{4}$$

which are the six lowest, above the $4s\ ^2S$ level. The pseudostates included will then be

$$\begin{aligned} &3d^2,\ 4p^2,\ 4d^2,\ 5p^2,\ 4f^2,\ 3d5s\ , \\ &3d4d,\ 4p5p,\ 4p4f,\ 5s4d,\ 5p4f \end{aligned} \tag{5}$$

and the channels will be

$$\begin{aligned} &3dns_1,\ 3dnd_1,\ 3dng_1,\ 4pnp_1,\ 4pnf_1,\ 5snd_2,\ 4dns_2 \\ &4dnd_3,\ 4dng_2,\ 5pnp_2,\ 5pnf_2,\ 4fnp_3,\ 4fnf_3,\ 4fnh_1\ . \end{aligned} \tag{6}$$

The subscript denotes the orthogonality restrictions. Only channel functions with the same subscript are constrained to be orthogonal. Channel functions belonging to CSF for different total LS are never required to be orthogonal. All are required to be orthogonal to target functions, which have no subscript.

Our model for the calcium atom (and ion) is improved and the important core polarization contributions are taken into account, by the inclusion of a model potential [18,19]

$$V_{\rm CP}(r)=-\frac{1}{2}\alpha_d\frac{r^2}{(r^2+r_c^2)^3}\ . \tag{7}$$

The α_d is the dipole polarizability, which is known theoretically to quite high accuracy. For calcium it is [20]

$$\alpha_d=3.254\ .$$

The cutoff radius r_c, however, can be chosen quite arbitrarily. In this work we adjust it to reproduce the experimental energy difference of $3d\ ^2D$ and $4p\ ^2P$ of Ca^+. The resulting value is

$$r_c=1.356\,27\ .$$

This approach is designed to get the best possible relative position of the Rydberg series, based on the $3d\ ^2D$ limit, and the perturbers, based on the $4p\ ^2P$.

A. The spline-Galerkin method

The B-spline basis [21,22] is introduced in our method through the expansion of the radial part $\bar{P}_{n_il_i}$ of the channel functions

$$\bar{P}_{n_il_i}(r)=\sum_{j=1}^{N}a_j(i)B_j(r)\ . \tag{8}$$

All through this work we are using B splines of order 8.

By inserting the approximate form of the ASF from Eq. (1) in the Schrödinger equation, we get

$$(\hat{H}-E)\Psi(\gamma LS)=\text{residual}\approx 0\ . \tag{9}$$

According to the Galerkin condition [23], the residual should be orthogonal to the solution space. To impose this, we need to choose a set of basis functions, so-called test functions τ, which spans our solution space. This set consists of all pseudostates

$$\tau^p(i)=\phi(\alpha_i LS)\quad \text{for } i=1,M_p \tag{10}$$

and "spline channels" obtained by exchanging the radial part of the channel functions for a B spline

$$\tau_j^c(i)=|(\text{target}_i\cdot B_j|l_is)^{(2S+1)}L\rangle \qquad \text{for } i=1,M_c;\ j=1,N\ . \tag{11}$$

The Galerkin conditions then leads to

$$\begin{aligned} &\langle\tau^p(i)|\text{residual}\rangle=0\quad \text{for } i=1,M_p \\ &\langle\tau_j^c(i)|\text{residual}\rangle=0\quad \text{for } i=1,M_c;\ j=1,N\ , \end{aligned}$$

which leads to a generalized eigenvalue problem of the form

$$(\mathbf{H}-E\mathbf{S})\mathbf{c}=0\ , \tag{12}$$

where $\mathbf{H}$ is the multichannel interaction matrix, as derived earlier [16,17], and $\mathbf{S}$ is the overlap matrix, consisting of diagonal blocks of the overlap matrix $\mathbf{B}$

$$B_{kl}=\langle B_k|B_l\rangle\ , \tag{13}$$

one for each channel. The $\mathbf{c}$ can be written

$$\mathbf{c}=\begin{vmatrix}\mathbf{c}^p\\ \mathbf{a}(1)\\ \mathbf{a}(2)\\ \vdots\\ \mathbf{a}(M_c)\end{vmatrix}\ , \tag{14}$$

where $\mathbf{c}^p$ is the column vector of pseudo coefficients

$$\mathbf{c}^p=(c(1),c(2),\ldots,c(M_p))^t \tag{15}$$

and each $\mathbf{a}(i)$ is a column vector of B-spline coefficient, according to Eq. (8), for the unnormalized, radial channel functions.

By this we can see that the form of our approximation leads to a linear problem that can be solved by standard procedures. Our choice of grid is based on the definition of grid points through the array t_i,

$$t_i=0 \quad \text{for } i=1,\ldots,k_s$$

$$t_{i+1}=\begin{cases} t_i+h & \text{for } i=k_s,\ldots,k_s+m,\quad m=1/h \\ t_i(1+h) & \text{for } h<t_{i+1}-t_i<h_{\max} \\ t_i+h_{\max} & \text{for } \dfrac{t_i}{Z}<r_{\max} \end{cases} \tag{16}$$

$$r_i=\frac{t_i}{Z} \quad \forall i \ .$$

We have found that in the case of bound states, the logarithmic grid is quite sufficient. Therefore, unless otherwise stated, we use the following grid parameters throughout this work:

$$h=0.125, \quad h_{\max}=r_{\max}=1000 \ .$$

A major complication, for the bound case, occurs when orthogonality conditions are applied on the radial channel functions, since it in principal destroys the eigenvalue character of the problem. This is solved by a transformation as suggested by Landtman *et al.* [24].

B. Orthogonality constraints

By using the spline-Galerkin method, the multichannel case with orthogonality constraints can be written

$$\begin{bmatrix} \mathbf{h}(pp)-EI & \mathbf{h}(1p)^t & \cdots & \mathbf{h}(M_cp)^t \\ \mathbf{h}(1p) & \mathbf{H}(11)-E\mathbf{B} & \cdots & \mathbf{H}(1M_c) \\ \mathbf{h}(2p) & \mathbf{H}(21) & \cdots & \mathbf{H}(2M_c) \\ \vdots & \vdots & \ddots & \vdots \\ \mathbf{h}(M_cp) & \mathbf{H}(M_c1) & \cdots & \mathbf{H}(M_cM_c)-E\mathbf{B} \end{bmatrix} \begin{bmatrix} \mathbf{c}_p \\ \mathbf{a}(1) \\ \mathbf{a}(2) \\ \vdots \\ \mathbf{a}(M) \end{bmatrix} + \begin{bmatrix} 0 \\ \sum_k \varepsilon(1k)\mathbf{B}\mathbf{b}(k) \\ \sum_k \varepsilon(2k)\mathbf{B}\mathbf{b}(k) \\ \vdots \\ \sum_k \varepsilon(M_ck)\mathbf{B}\mathbf{b}(k) \end{bmatrix} = 0 \ , \tag{17}$$

where the $\mathbf{H}(ij)$'s are the matrices describing interaction between different "channels." The $\mathbf{h}(ip)$'s represent the interaction between a channel and the different pseudostates and $\mathbf{h}(pp)$ is the pseudo-pseudointeraction. The $\mathbf{b}(k)$ column vectors constitute the expansions for different constraining functions and $\varepsilon(ik)$ is a Lagrange multiplier that is nonzero only if the solution vector $\mathbf{a}(i)$ is constrained to be orthogonal to $\mathbf{b}(k)$.

Again, Eq. (17) is transformed to an eigenvalue problem

$$(\mathbf{H}'-E\mathbf{S})\mathbf{c}=0 \ , \tag{18}$$

where

$$\mathbf{H}'(ij)=\mathbf{H}(ij)-\sum_{k;\varepsilon(ik)\neq 0}\mathbf{B}\mathbf{b}(k)\circ\mathbf{b}(k)'\mathbf{H}(ij)$$

$$\text{for } j=1,\ldots,M_c \ , \tag{19}$$

i.e., a whole "superrow" for channel i is transformed for each orthogonality. Spurious zero solutions will turn up for each $\mathbf{b}(k)$ introduced. The matrix $\mathbf{H}'$ is not symmetric any longer, but all eigenpairs are still real. We use the RGG routine of EISPACK [25] to find the eigenvalues of the $\mathbf{H}'$ matrix and inverse interation to find the corresponding eigenvectors.

C. Breit-Pauli CI

The solutions obtained from the spline-Galerkin calculations, as given in Eq. (1), can be used for a CI-type calculation including the Breit-Pauli operators [26,27]. In this model the atomic state function $\Psi(\gamma J)$ is a linear combination of (LS)-dependent functions

$$\Psi(\gamma J)=\sum_{LS}\sum_{k=1}^{N_{LS}}\sigma_k(LSJ)\Psi_k(\gamma LSJ) \ , \tag{20}$$

where the $\Psi_k(\gamma LSJ)$'s are a set of solutions from the spline-Galerkin calculations, one set for each allowed LS value. The basis functions for this CI type of calculation are given by Eq. (1). The details of this method are outlined by Brage and Froese Fischer [16]. The CI matrix will consist of blocks, one for each pair of LS values. Standard Racah algebra methods [26] are used to find the angular coefficients, while the different radial integrals appear as matrices (describing channel-channel interaction), vectors (pseudochannel interaction), and scalars (pseudo-pseudointeraction), which have to be folded into the interaction matrix.

III. RESULTS

The even Rydberg series between the $4s\ ^2S$ and $3d\ ^2D$ limits are of the form $3dnl\ ^{1,3}L$ and possible perturbers are built on the $4p\ ^2P$ limit. For some values of LS there are a number of different interleaved series and the presence of a perturber enhances the complexity of this system. To analyze these series and detect irregularities, we will use two properties. First, the effective quantum number n^* is defined according to

$$E_B(\text{limit})=\frac{(Z-N+1)^2}{n^*(\text{limit})^2} \tag{21}$$

and the quantum defect is defined as

$$\delta(\text{limit})=n-n^*(\text{limit}) \ , \tag{22}$$

where E_B is the binding energies relative to a given limit, Z is the atomic number, and N is the number of electrons. It is important to notice that the effective quantum number and the quantum defect are dependent on which limit is used to define the binding energy.

To show the irregularities introduced by perturbers, we will plot the quantum defect with respect to the second $3d$ limit, $\delta(3d)$, as a function of the effective quantum number with respect to the third $4p$ limit, $n^*(4p)$. The latter is then basically just an energy scale.

A. Nonrelativistic results

The first step is to generate results for all different LS terms of interest. Our aim is to investigate states with $J=0-3$, so for completeness we need to include ^3G, ^3F, ^1F, ^3D, ^1D, ^3P, ^1P, ^3S, and ^1S. They all have different behaviors, depending on the number of interleaved Rydberg series and the presence of perturbers, so let us discuss them one at a time.

1. $^3G^e$

The set of pseudostates included in this case is $3d4d$, $4p4f$, and $5p4f$ and the set of channels is $3dnd_1$, $3dng_1$, $3dni_1$, $4pnf_1$, $4pnh_1$, $5sng_2$, $4dnd_2$, $4dng_3$, $4dni_2$, $5pnf_2$, $5pnh_2$, $4fnp_1$, $4fnf_3$, $4fnh_3$, and $4fnk_1$. There are three different interleaved series present, namely, $3dnd$, $3dng$, and $3dni$. As can be seen in Fig. 1, the behavior of these series is very regular and no perturber is detected.

2. $^3F^e$

For this symmetry we include the pseudostates $3d^2$, $4d^2$, $4f^2$, $3d4d$, $4p4f$, and $5p4f$ and the channels $3dnd_1$, $3dng_1$, $4pnf_1$, $4dnd_2$, $4dng_2$, $5pnf_2$, $4fnp_1$, $4fnf_3$, and $4fnh_1$. In this case there are two interleaved Rydberg series $3dnd$ and $3dng$. Again, no perturber could be detected.

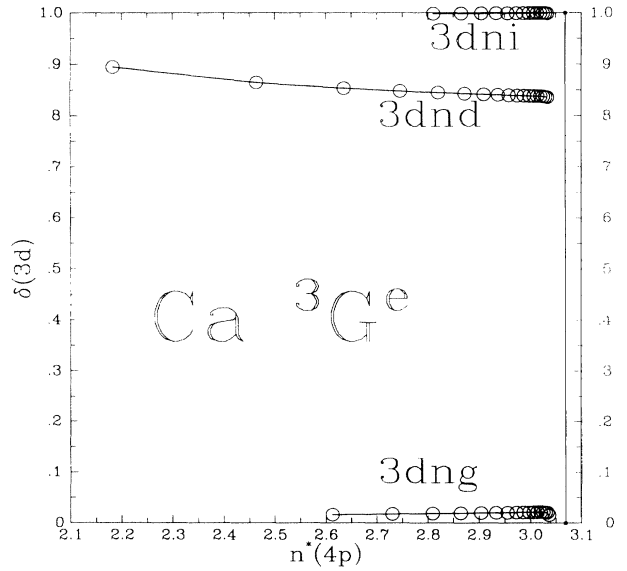

FIG. 1. The quantum defect with respect to the $3d$ limit, as a function of the effective quantum number with respect to the $4p$ limit, for the $^3G^e$ terms above the $4s\ ^2S$ limit of neutral calcium. The results are from the nonrelativistic calculation with $r_{max}=1000$ a.u. (see text). The vertical line represent the position of the $3d\ ^2D$ limit.

3. $^1F^e$

The $^1F^e$ is very similar to $^3F^e$. The same channels are included and the three pseudochannels that will couple to a $^1F^e$ are $3d4d$, $4p4f$, and $5p4f$. The $n^*(4p)/\delta(3d)$ plot is almost identical to the $^3F^e$, with the $3dnd$ and $3dng$ Rydberg series and no perturbers.

4. $^3D^e$

Considerably more interesting is the $^3D^e$ series. The set of pseudostates used are $3d5s$, $3d4d$, $4p5p$, $4p4f$, $5s4d$, and $5p4f$ while the channels included are $3dns_1$, $3dnd_1$, $3dng_1$, $4pnp_1$, $4pnf_1$, $5snd_2$, $4dns_2$, $4dnd_3$, $4dng_2$, $5pnp_2$, $5pnf_2$, $4fnp_3$, $4fnf_3$, and $4fnh_1$. Again we have three interleaved series $3dns$, $3dnd$, and $3dng$, but from Fig. 2 it is obvious that a perturber is present. By examining the total weights of different symmetries, it is clear that this perturber should be labeled $4p5p\ ^3D$. In Fig. 2 we have also indicated the total weight of the $4pnp$ CSF (that is, $4p5p$ and $4pnp_1$), for some states around the perturber. It is clear that no single state has a major component of $4pnp$ character, but that the perturber is rather spread out over, predominantly, the $3dns$ and $3dnd$ series. We will return to this when looking at the relativistic results.

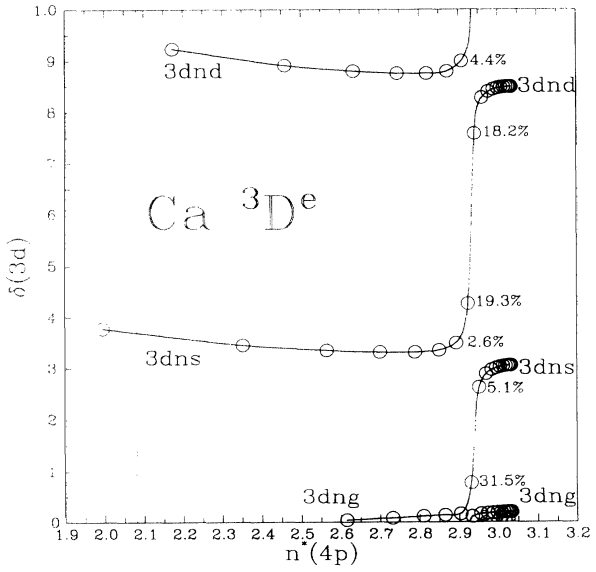

FIG. 2. The quantum defect with respect to the $3d$ limit, as a function of the effective quantum number with respect to the $4p$ limit, for the $^3D^e$ symmetry above the $4s\ ^2S$ limit of neutral calcium. The results are from the nonrelativistic calculations with $r_{max}=1000$ a.u. (see text). The vertical dashed line represents the position of the $4s\ ^2S$ limit. The numbers represent the percentage of $4pnp$ (including $4p5p$ and $4pnp_1$) character for different "perturbed" states.

5. $^1D^e$

For the $^1D^e$ case we include the same pseudostates and channels as for $^3D^e$, with the addition of the "equivalent electron" pseudostates $3d^2$, $4p^2$, $4d^2$, $5p^2$, and $4f^2$. This series is our first example when $4p^2$ is the lowest perturber. This leads to a much lower perturbation than for the $^3D^e$ case, as can be seen in Fig. 3. The perturber is well below the $4s\ ^2S$ limit, as represented by the vertical dashed line in this figure.

6. $^3P^e$

With the $L=1$ and 0 cases, we have only one series, the $3dnd$ series. The perturber situation is quite different in the four different cases though. For the $^3P^e$ we again have a somewhat similar situation as for the $^1D^e$.

The lowest perturber is $4p^2$ and we first find no trace of a $4p5p$ perturber. To further investigate the possibility of a bound $4p5p\ ^3P^e$ perturber, we perform a somewhat larger calculation, with $r_{\max}=5000$ and $h_{\max}=500$. The results from this are shown in Fig. 4. The quantum defect is rapidly increasing close to the limit, which indicates a perturber close to it.

To deduce whether the $4p5p\ ^3P^e$ is below or above the $3d\ ^2D$ limit, we investigate the total weight of the $4pnp$ CSF (that is, $4p^2$, $4p5p$, and $4pnp_1$). In Fig. 5 we give the accumulative value of this weight

$$C_N^2(4pnp)=\sum_i^N c_i^2(4pnp)$$

(that is, for a certain state N it is the sum of the weights of $4pnp$ for all states below the Nth level). We can see that even though the weight c_i^2 is decreasing for higher Rydberg members, and no state above the third has a weight of $4pnp$ larger than 0.005, the accumulative

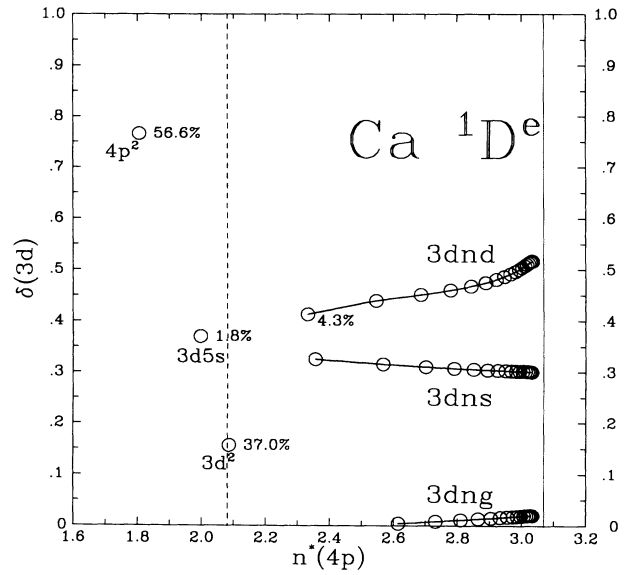

FIG. 3. The quantum defect with respect to the $3d$ limit, as a function of the effective quantum number with respect to the $4p$ limit, for the $^1D^e$ symmetry above the $4s\ ^2S$ limit of neutral calcium. The results are from the nonrelativistic calculations with $r_{\max}=1000$ a.u. (see text). The vertical dashed and solid lines represent the position of the $4s\ ^2S$ and $3d\ ^2D$ limits, respectively. The numbers represents the percentage of $4pnp$ (including $4p^2$, $4p5p$, and $4pnp_1$) character for different perturbed states.

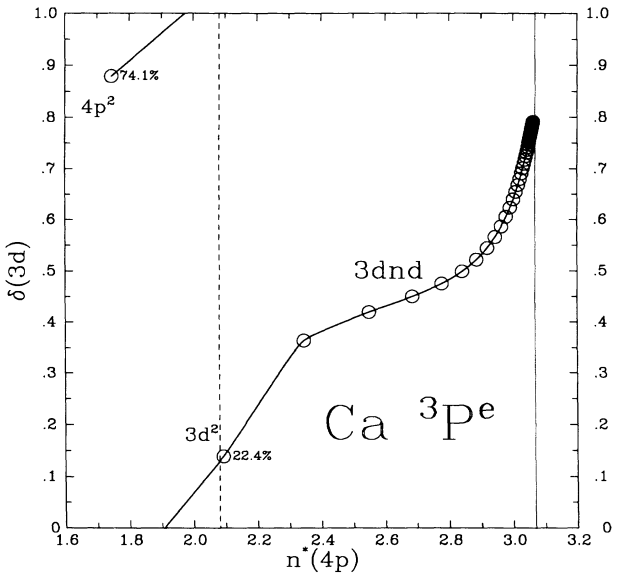

FIG. 4. The quantum defect with respect to the $3d$ limit, as a function of the effective quantum number with respect to the $4p$ limit, for the $^3P^e$ symmetry above the $4s\ ^2S$ limit of neutral calcium. The results are from the nonrelativistic calculations with $r_{\max}=5000$ a.u. (see text). The vertical dashed and solid lines represent the position of the $4s\ ^2S$ and $3d\ ^2D$ limits, respectively. The numbers represents the percentage of $4pnp$ (including $4p^2$, $4p5p$, and $4pnp_1$) character for different perturbed states.

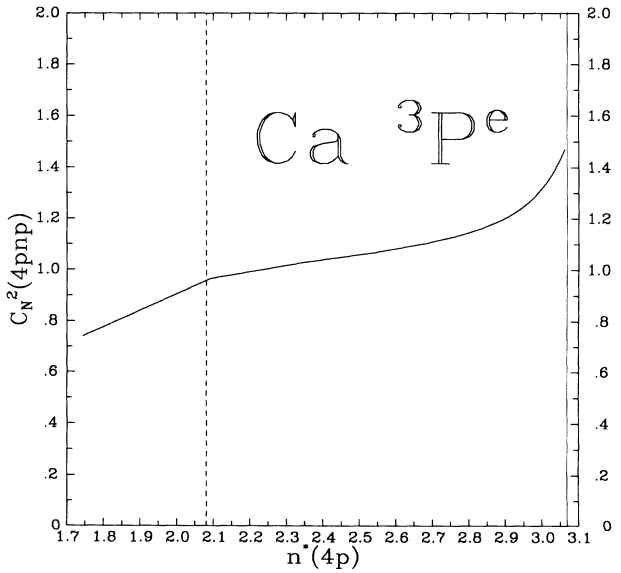

FIG. 5. The accumulative weight $C_N^2(4pnp)=\sum_i^N c_i^2(4pnp)$ of $4pnp$ for the $^3P^e$ symmetry above the $4s\ ^2S$ limit of neutral calcium. The results are from the nonrelativistic calculations with $r_{\max}=5000$ a.u. (see text). The vertical dashed and solid lines represent the position of the $4s\ ^2S$ and $3d\ ^2D$ limits, respectively.

weight increases and seems to converge to a point very close to 1.5. This is the most extreme case of a perturber spread out over a Rydberg series known to the authors. The question whether a second $4pnp\ ^3P^e$ state ($4p5p\ ^3P^e$) is bound or not is still left open and might be a matter of definition.

For all the $^3P^e$ calculations the pseudostates included are $3d^2$, $4p^2$, $4d^2$, $5p^2$, $4f^2$, $3d4d$, and $4p5p$ and we use the five channels $3dnd_1$, $4pnp_1$, $4dnd_2$, $5pnp_2$, and $4fnf_1$.

7. $^1P^e$

This symmetry can be predicted to give the lowest member of the $4p5p$ configuration, which is confirmed by our calculations. The pseudostates and channels included are $3d4d$, $4p5p$, $3dnd_1$, $4pnp_1$, $4dnd_2$, $5pnp_2$, and $4fnf_1$. The resulting behavior of the quantum defect is given in Fig. 6 and the behavior of the accumulative weight of $4pnp$ is given in Fig. 7. The perturber in this case is quite localized to just a few states. It is also clear that there is no other perturber even close to the limit.

8. $^3S^e$

This LS symmetry symmetry has large similarities with $^1P^e$, starting with the fact that the sets of CSF's are the same. The $^3S^e$ could be the third to fifth lowest term in the $4p5p$ configuration (clearly above the $^1P^e$ and $^3D^e$, but below $^1S^e$). From a similar analysis of this state as for $^3P^e$ we can see that the perturber is clearly above the limit and further away than for the $^3P^e$ case. The accumulative weight of $4pnp\ ^3S^e$ seems in this case to be converging to about 0.2–0.3.

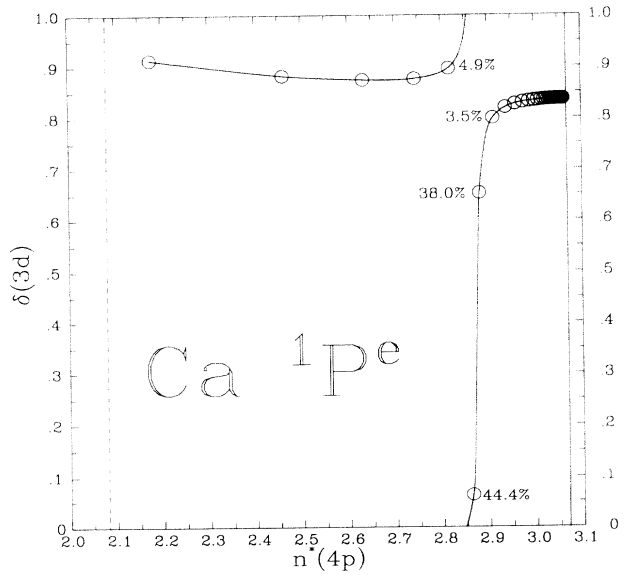

FIG. 6. The quantum defect with respect to the $3d$ limit, as a function of the effective quantum number with respect to the $4p$ limit, for the $^1P^e$ symmetry above the $4s\ ^2S$ limit of neutral calcium. The results are from the nonrelativistic calculations with $r_{max}=5000$ a.u. (see text). The vertical dashed and solid lines represent the position of the $4s\ ^2S$ and $3d\ ^2D$ limits, respectively. The numbers represent the percentage of $4pnp$ (including $4p5p$ and $4pnp_1$) character for different perturbed states.

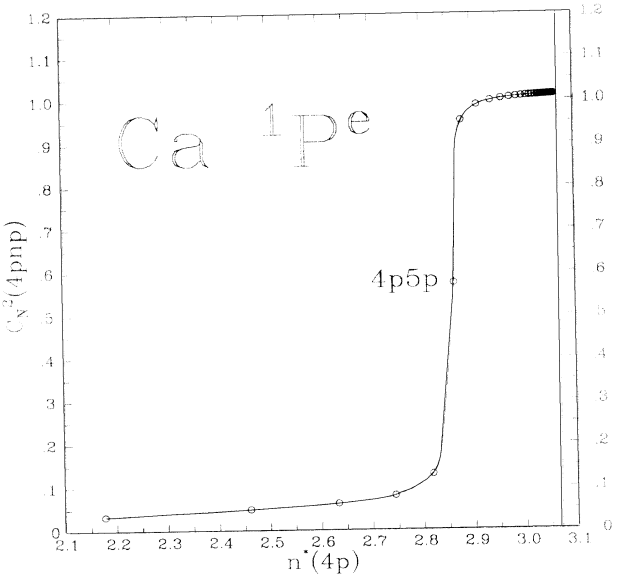

FIG. 7. The accumulative weight $C_N^2(4pnp)=\sum_i^N c_i^2(4pnp)$ of $4pnp$ for the $^1P^e$ symmetry above the $4s\ ^2S$ limit of neutral calcium. The results are from the nonrelativistic calculations with $r_{max}=5000$ a.u. (see text). The vertical solid line represents the position of the $3d\ ^2D$ limit.

9. $^1S^e$

The $^1S^e$ presents us with one difficult choice, concerning the treatment of the $4s^2\ ^1S^e$ CSF. We choose to include it in our calculation and not treat it as a member of the deleted $4sns\ ^1S^e$ series. We expect that this will give a larger uncertainty for this series.

The pseudochannels included are $4s^2$, $3d^2$, $4p^2$, $5s^2$, $4d^2$, $5p^2$, $4f^2$, $3d4d$, and $4p5p$ and the channels are $5sns_1$, $3dnd_1$, $4pnp_1$, $4dnd_2$, $5pnp_2$, and $4fnf_1$. There has been a discussion of whether the $3d^2\ ^1S^e$ level or the $4p^2\ ^1S^e$ level is the lowest state in this series (see [1,4] and references therein). Of course, the answer is somewhat a matter of taste, but by looking at Fig. 8 we can see that even though almost 42% of the $4pnp$ (including $4p^2$) is present in the second lowest state and over 70% is spread out over the third to the eighth states. It is also in the latter region that the behavior of the quantum defect most resembles a case with a perturber. $3d^2$, being the lowest member of the $3dnd$ series, is in principle not a perturber. We therefore recommend the naming convention suggested before [5] where the second state is $3d^2\ ^1S^e$ and the fifth is $4p^2\ ^1S^e$. It is also clear that this symmetry does not support any second "bound" perturber, below the $3d$ limit, since the accumulative weight $C_N^2(4pnp)$ approaches 1.3.

10. Summary

By investigating all the different LS series, which can give levels with J values ranging from 0 to 3, we have found that the $^3P^e$, $^1D^e$, and $^1S^e$ states have the expected $4p^2$ perturber. The lowest term of the $4p5p$ configuration is without any doubt the $^1P^e$, followed by $^3D^e$. Both these

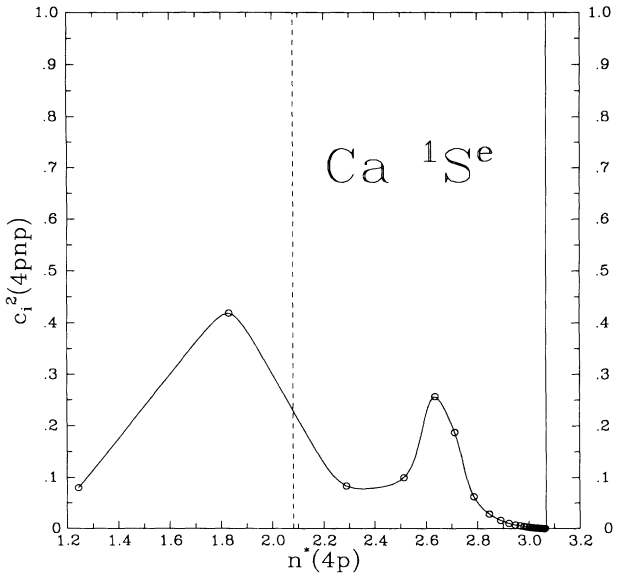

FIG. 8. Weight of $4pnp$ (that is, the total weight of $4p^2$, $4p5p$, and $4pnp_1$) for the $^1S^e$ symmetry above the $4s\ ^2S$ limit of neutral calcium. The results are from the nonrelativistic calculations with $r_{max}=5000$ a.u. (see text). The vertical dashed and solid lines represent the position of the $4s\ ^2S$ and $3d\ ^2D$ limits, respectively.

are clear perturbers in the corresponding $3dnl$ series. The next candidate to be below the $3d$ limit seems to be $^3P^e$, which in our calculation is present to 50% in the $3dnd\ ^3P^e$ series. The $^3S^e$ and $^1S^e$ states are clearly not supporting any $4p5p$ perturber, since the accumulative weight for the $4pnp$ series approaches 0.3 and 1.3, respectively, in these two cases.

B. Relativistic results

The different LS series obtained from the spline-Galerkin calculations were used in a Breit-Pauli CI type of approach for $J=0$–3. Some of the most interesting energy levels, for $J=0$, 1, and 3, are given in Tables I–III, together with the LS and configuration composition. It is clear that LS coupling is only good for low n, and for higher members of the series the coupling approaches jK coupling.

1. $J=0$

Our first example is the $J=0$ states. There are only two different LS symmetries, which give this J value, ^3P and ^1S. The resulting energies and compositions are given in Table I. The jK-coupled case corresponds here to mixing coefficients of 0.6 and 0.4, which is the behavior we observe for high n.

There are two other results to compare with in this case: first the experimental work by Bolovinos *et al.* [9] and second the R-matrix calculations by Aymar and Telmini [5]. The latter do not include relativistic effects in an *ab initio* manner. Instead only the energy difference of the two fine-structure levels of the limit is included, together with a transformation for LS-coupled results to a jj-coupling scheme. A more thorough comparison between our results and these is made in a separate paper, where also some experimental results are reported [28]. As shown there, the agreement is quite satisfactory both with the very accurate R-matrix theory and the different experimental results.

2. $J=1$

More interesting than $J=0$, from a theoretical point of view, are the $J=1$ levels. In this case we have four contributing LS series ^3D, ^3P, ^3S, and ^1P. We have already seen that both ^3D and ^1P contain a perturber and the ^3P probably has one not too far from the limit. The resulting energies and compositions are given in Table II.

In Fig. 9 we show the "$4pnp$-composition spectra" as a function of the number of the eigenvalue. The first few high values correspond to the $4p^2\ ^3P_1$ perturber, while the first tall narrow peak at eigenvalue number 32 is $4p5p\ ^1P_1$. Both these are quite concentrated, with one eigenvalue containing more than 50% of the $4pnp$ character. The $^3D_1$ state, however, is spread out over a number of eigenvalues, represented by the cluster of shorter peaks around eigenvalue 35–45. Not obvious from this figure is the presence of the $4p5p\ ^3P_1$ and, possibly, $^3S_1$ close to the limit. This is obvious, however, in Fig. 10, where we show the accumulative weight of $4pnp$, $C_N^2(4pnp)$, as a function of $n^*(4p)$. The span of the different perturbers are clearly seen, in an energy scale: first the broad $4p^2$

TABLE I. Excitation energies, term compositions, and configuration compositions (in %) of $J=0$, even states of calcium, above the $4s\ ^2S$ limit. The excitation energies are computed with the assumption that the energy difference of the $4s^2\ ^1S$ and the $3d\ ^2D$ limit is 62 992.564 cm^{-1}.

Energy (cm^{-1})	Label	Term comp. ^3P	Term comp. ^1S	Config. comp. $4s^2$	Config. comp. $3dnd$[a]	Config. comp. $4pnp$[b]
2 892.86[c]	$4s^2$	0.00	100.00	91.55	0.46	7.88
38 445.47[c]	$4p^2$	99.94	0.06	0.00	24.95	74.65
41 875.27[c]	$3d^2$	0.07	99.93	1.59	55.52	42.16
49 532.25	$3d^2$	99.98	0.01	0.00	77.45	21.83
53 673.17	$3d4d$	0.13	99.87	0.48	90.65	8.36
54 671.04	$3d4d$	99.86	0.14	0.00	93.51	6.29
57 267.41	$3d5d$	0.23	99.77	0.45	88.50	10.08
57 738.99	$3d5d$	99.63	0.37	0.00	95.54	4.36
58 833.83	$4p^2$	0.18	99.82	0.49	71.29	25.98
59 400.78	$3d6d$	98.14	1.86	0.00	95.86	4.05
59 719.76	$3d6d$	1.82	98.18	0.11	80.75	17.91
60 378.35	$3d7d$	89.73	10.27	0.00	96.30	3.62
60 527.26	$3d7d$	10.29	89.71	0.00	93.97	5.75
60 999.75	$3d8d$	82.54	17.46	0.00	97.08	2.88
⋮						
62 340.81	$3d14d$	64.80	35.20	0.00	99.35	0.64
62 409.82	$3d14d$	51.02	48.98	0.00	98.25	1.73
62 427.59	$3d15d$	47.86	52.14	0.00	99.71	0.28
62 479.87	$3d15d$	62.17	37.83	0.00	98.65	1.34

[a]Sum over all $3d^2$, $3d4d$, and $3dnd$ components.
[b]Sum over all $4p^2$, $4p5p$, and $4pnp$ components.
[c]State below the $4s\ ^2S$ components.

TABLE II. Excitation energies, term compositions, and configuration compositions (in %) for $J=1$, even levels in neutral calcium, above the $4s\ ^2S$ limit. The energies are computed with the assumption of a $3d\ ^2D$ limit energy of 62 992.564 cm^{-1}.

Energy		Term comp.				Config. comp.			
(cm^{-1})	Label	^3D	^3P	^3S	^1P	$3dns$[a]	$3dnd$[b]	$3dng$[c]	$4pnp$[d]
⋮									
61 034.61	$3d8d$	0.68	97.32	1.83	0.17	0.00	97.08	0.00	2.89
61 074.18	$3d10s$	99.83	0.00	0.00	0.17	98.66	0.12	0.01	1.17
61 202.57	$4p5p$	7.09	0.05	1.33	91.53	0.57	47.43	0.01	51.75
61 302.07	$3d9d$	90.78	1.39	0.77	7.07	0.07	80.67	12.37	6.81
61 303.56	$3d8g$	98.77	0.18	0.05	1.01	0.00	11.68	87.35	0.83
61 330.52	$3d9d$	0.43	4.38	85.39	9.79	0.06	93.52	0.02	6.37
61 398.66	$3d9d$	6.25	0.20	8.52	85.03	1.05	80.50	0.02	18.32
61 461.55	$3d9d$	2.89	92.41	4.15	0.56	1.18	95.91	0.00	2.87
61 475.41	$3d11s$	97.08	1.11	0.00	1.80	92.30	2.94	0.03	4.63
61 622.71	$3d10d$	89.25	0.79	0.40	9.56	3.82	81.11	0.39	14.40
61 656.58	$3d10d$	12.33	7.19	54.12	26.37	1.95	87.55	4.58	5.77
61 664.44	$3d9g$	94.21	0.90	4.57	0.32	0.06	7.04	92.61	0.15
61 693.75	$4p5p$	50.56	3.71	21.51	24.22	15.50	55.72	2.12	26.14
61 729.31	$3d10d$	45.92	2.56	12.24	39.28	17.30	69.78	0.23	12.45
61 765.23	$3d10d$	8.07	83.17	7.27	1.49	4.46	93.42	0.00	2.10
61 800.36	$3d12s$	96.64	1.61	0.02	1.73	68.72	11.88	0.13	18.89
⋮									

[a]Sum over all $3d5s$ and $3dns$ components.
[b]Sum over all $3d^2$, $3d4d$, and $3dnd$ components.
[c]Sum over all $3dng$ components.
[d]Sum over all $4p^2$, $4p5p$, and $4pnp$ components.

TABLE III. Excitation energies, term compositions, and configuration compositions (in %) for $J=3$, even levels in neutral calcium, above the $4s\ ^2S$ limit. The energies are computed with the assumption of a $3d\ ^2D$ limit energy of 62 992.564 cm^{-1}.

Energy		Term comp.				Config. comp.				
(cm^{-1})	Label	^3G	^3F	^3D	^1F	$3dns$[a]	$3dnd$[b]	$3dng$[c]	$3dni$	$4pnp$[d]
⋮										
61 702.12	$3d10d$	3.73	0.31	53.08	42.88	0.76	96.01	0.05	0.00	3.12
61 779.96	$3d10d$	1.45	89.11	4.62	4.82	0.81	97.59	0.03	0.00	1.53
61 820.74	$3d12s$	0.04	2.35	97.40	0.20	63.92	9.80	2.16	0.00	23.55
61 843.26	$3d10g$	55.03	19.06	0.00	25.90	0.00	0.01	99.94	0.00	0.00
61 844.01	$3d10g$	0.00	19.17	66.81	14.02	2.28	0.04	97.50	0.00	0.11
61 880.10	$3d11d$	70.58	0.22	8.64	20.57	2.50	96.54	0.04	0.00	0.89
61 895.37	$4p5p$	16.57	4.80	74.74	3.89	25.23	55.58	0.70	0.00	18.12
61 919.89	$3d11d$	7.65	17.61	30.23	44.51	9.02	58.13	20.83	0.00	11.70
61 922.32	$3d10g$	44.87	20.61	0.09	34.43	0.00	0.02	99.91	0.02	0.00
61 923.47	$3d10g$	1.65	32.86	35.88	29.61	2.83	14.09	78.69	0.00	4.31
61 927.06	$3d10i$	99.99	0.00	0.00	0.01	0.00	0.00	0.02	99.98	0.00
61 968.54	$3d11d$	1.77	2.88	73.25	22.10	6.42	82.18	0.28	0.00	10.88
62 003.38	$3d11d$	2.07	81.21	11.15	5.57	1.32	97.28	0.06	0.00	1.30
62 034.74	$3d11g$	54.99	19.07	0.00	25.94	0.00	0.01	99.95	0.00	0.00
62 035.20	$3d11g$	0.00	19.48	66.30	14.22	0.15	0.06	99.64	0.00	0.09
62 063.10	$3d12d$	76.92	0.07	4.95	18.07	2.60	97.37	0.01	0.00	0.01
62 070.60	$3d13s$	3.86	0.68	95.40	0.05	88.00	8.03	0.01	0.00	3.80
⋮										

[a]Sum over all $3d5s$ and $3dns$ components.
[b]Sum over all $3d^2$, $3d4d$, and $3dnd$ components.
[c]Sum over all $3dng$ components.
[d]Sum over all $4p^2$, $4p5p$, and $4pnp$ components.

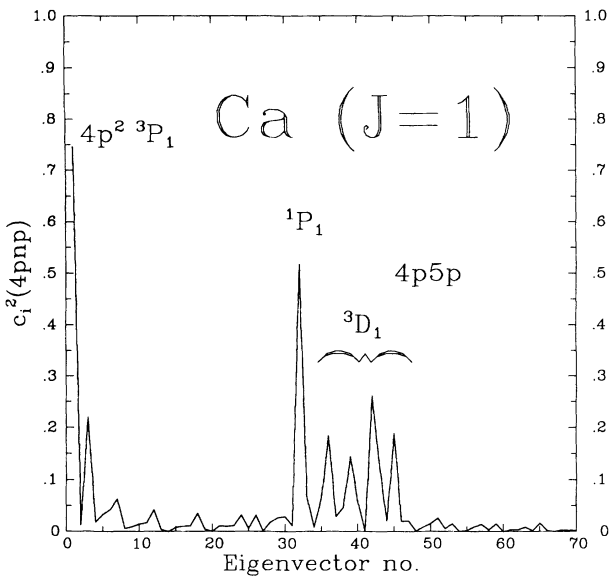

FIG. 9. Weight of $4pnp$ (that is, the total weight of $4p^2$, $4p5p$, and $4pnp_1$) for the $J=1$ levels above the $4s\ ^2S$ limit of neutral calcium, as a function of eigenvalue number. The results are from the CI Breit-Pauli calculations with $r_{max}=5000$ a.u. (see text).

and second the $4p5p$ over a smaller energy range, but spanning up to the limit.

3. $J=2$

For this J value, the possible LS symmetries are ^3F, ^3D, ^3P, and ^1D. The perturbers, as predicted from the nonrelativistic calculation, should be $4p^2\ ^3P$, ^1D, and $4p5p\ ^3D$.

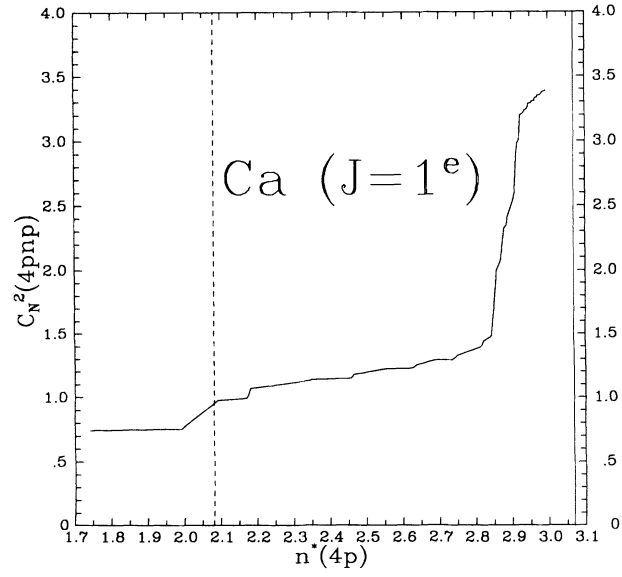

FIG. 10. The accumulative weight $C_N^2(4pnp)=\sum_i^N c_i^2(4pnp)$ of $4pnp$ for the $J=1$ levels above the $4s\ ^2S$ limit of neutral calcium. The results are from the CI Breit-Pauli calculations. The dashed and solid lines represent the position of the $4s\ ^2S$ and $3d\ ^2D$ limits, respectively.

There exist experimental and other theoretical values for this J value, from the same sources as for $J=0$ [9,5]. The agreement between our calculations and the older results is again quite good [28].

4. $J=3$

For $J=3$ there is again one perturber present, the $4p5p\ ^3D_3$. The resulting energies are given in Table III.

IV. SUMMARY

We have combined the recently introduced spline-Galerkin method with a Breit-Pauli CI approach, to investigate the structure of even levels above the $4s\ ^2S$ limit of calcium. The main Rydberg series are based on the $3d$ limit and are of the form $3dnl$. Perturbers appear through the lowest members of Rydberg series based on even higher limits, in this case the $4p\ ^2P$. By first investigating the different series in a nonrelativistic approach, we could deduce which perturbers could be expected to appear beneath the $3d\ ^2D$ limits and which ones are not "bound." Interaction between different LS series is included through a final, relativistic, J-dependent calculation, since the LS approximation breaks down for higher n values. This is due to the fact that while the electrostatic interaction between the outer nl electron and the inner $3d$ decreases, the spin-dependent interactions are fairly constant since they are induced by the common $3d$ electron. The involvement of configurations with the $4p$ occupied will induce even stronger mixing. As we can see from the different tables, the LS coupling breaks down quite early in the series. The best way of describing these states would probably be in a jK-coupling scheme. At the same time, the perturbers $4p^2$ and $4p5p$ consist of two inner electrons and are quite accurately described by the LS coupling.

The influence of a certain perturber on a Rydberg series can appear in many different ways. Sometimes the interaction between the series and the perturber is quite weak and there is clearly one particular level that should be designated to the perturber. At other times the interaction is strong and the influence of the perturber is spread out over a large number of levels. In the latter case it is clear that the identification of one certain label as the perturber is mainly a matter of convenience.

We have seen in our examples how different perturbers can be detected from quantum defect analyses. We have also seen that a way to determine whether a certain perturber is below the limit or not is to investigate the "accumulative weight" over the Rydberg series. Every time it increases by more than one unit we have another complete bound perturber. The three lowest terms of $4p5p$ illustrate these points perfectly. First the quite weak interaction between the $4p5p\ ^1P_1$ and the $3dnd$ Rydberg series gives a localized perturber. One level has more than 50% $4pnp$ character, as can be seen from Table II, and the labeling is unproblematic. When it comes to the $4p5p\ ^3D$ levels, the situation is much more complicated. We have indicated this in Table IV by giving a range of the influence of certain perturbers. There is no single state, for any of the three J values, that has more than

TABLE IV. The excitation energy (in cm^{-1}, above the $4s^2\,{}^1S$ ground state) of different perturbers of the even Rydberg series of calcium. The lower and upper limits of the range give the excitation energy of the lowest and highest energy levels that have more than 10% of the perturber character. The experimental values are from Sugar and Corliss [29] and Bolovinos *et al.* [9].

		Present			
		Nonrelativistic	Relativistic	Range	
Level	Experiment			Lower limit	Upper limit
$4p^2\,{}^3P_0$	38 417.543	38 593.74	38 445.47		
$4p^2\,{}^3P_1$	38 464.808	38 593.74	38 481.49		
$4p^2\,{}^3P_2$	38 551.558	38 593.74	38 547.97		
$4p^2\,{}^1D_2$	40 719.847	40 996.26	40 938.64		
$3d^2\,{}^1S_0$	41 786.276	41 924.80	41 875.27		
$3d^2\,{}^3F_2$	43 474.827	44 344.24	44 316.56		
$3d^2\,{}^3F_3$	43 489.119	44 344.24	44 339.12		
$3d^2\,{}^3P_0$	48 524.093	49 584.41	49 532.25		
$3d^2\,{}^3P_1$	48 537.623	49 584.41	49 552.18		
$3d^2\,{}^3P_2$	48 563.522	49 584.41	49 583.07		
$3d^2\,{}^1D_2$		49 420.20	49 383.91		
$4p^2\,{}^1S_0$	58 535	58 850.11	58 833.83	57 267.41	59 719.76
$4p5p\,{}^1P_1$		61 250.49	61 202.57	61 202.57	61 398.66
$4p5p\,{}^3D_1$		61 877.81	61 693.75	61 622.71	61 800.36
$4p5p\,{}^3D_2$	61 919.7	61 877.81	61 740.79	61 740.79	61 806.57
$4p5p\,{}^3D_3$		61 877.81	61 895.37	61 820.74	61 968.54

30% of the perturber character. The actual naming of the perturber has here been done by also looking at the trend along the series for different terms. The ambiguity in the identification of this perturber has to be remembered when comparing the present results with other theories and experiment. For the $4p5p\,{}^3P$ levels, finally, the position is, if below the $3d$ limit at all, so high in the corresponding Rydberg series that its width will span a large number of Rydberg states. It is therefore completely diluted in the series and could not be detected by investigating the composition of a single Rydberg state at a time. Instead we have to look at the accumulative weight or the quantum defect trends.

We have listed all the detected perturbers, together with the $3d^2$ levels, in Table IV. For the second configuration built on the $4p$ limit, $4p5p$, we detect four perturbers below the limit, $^1P_1$ and $^3D_{1,2,3}$. The ^3P_J levels might, to more than 50%, be below the $3d$ limit, but our calculations cannot detect this with a large certainty. It is quite clear, though, that the $4p5p\,{}^3S$, ^1D, and ^1S levels are all above the limit.

Our results agree quite well with other theories [5] and experiments [9], especially considering the uncertainties introduced by two different approximations. First, compared to the R-matrix calculation by Aymar and Telmini, we use a very simple approximation for the core-polarization potential, with only one adjustable parameter (compared to their 16 parameter potential). Second, we do exclude the effect of the $4snl$ series and continuum. This makes the results for all states below the $4s$ limit quite unreliable and it also excludes the possible energy shift from interaction with the continuum. On the other hand, the present work includes the Breit-Pauli interaction explicitly to describe the mixing of terms. A detailed comparison between our results and others has been done elsewhere [28].

ACKNOWLEDGMENTS

We are grateful to Professor T. Lucatorto for suggesting the study of this system. This research was supported by Division of Chemical Sciences, Office of Basic Energy Sciences, Office of Energy Research, U.S. Department of Energy.

[1] C. Froese Fischer and J. E. Hansen, J. Phys. B **18**, 4031 (1985).
[2] T. Brage, C. Froese Fischer, M. Godefroid, N. Vaeck, and A. Hibbert, Phys. Scri. **48**, 533 (1993).
[3] N. Vaeck, M. Goidefroid, and J. E. Hansen, J. Phys. B **24**, 361 (1991).
[4] T. Brage and C. Froese Fischer, Phys. Scr. **49**, 651 (1994).
[5] M. Aymar and M. Telmini, J. Phys. B **24**, 4935 (1991).
[6] M. J. Seaton, Rep. Prog. Phys. **46**, 976 (1983).
[7] U. Fano and A. R. P. Rau, *Atomic Collisions and Spectra* (Academic, Orlando, 1986).
[8] C. H. Greene and Ch. Jungen, Adv. At. Mol. Phys. **21**, 51 (1985); C. H. Greene, Phys. Rev. A **32**, 1880 (1985).
[9] A. Bolovinos, A. Jimoyiannis, S. Assimopoulos, and P. Tsekeris, J. Phys. B **25**, L533 (1992).
[10] G. H. Newsom, Proc. Phys. Soc. London **87**, 975 (1966).
[11] J. Karamatskos, M. Muleeler, M. Schmidt, and P. Zimmerman, J. Phys. B **18**, L107 (1985).
[12] J. O. Gaardsted, T. Andersen, H. K. Haugen, J. E. Hansen, and N. Vaeck, J. Phys. B **24**, 4363 (1991).

[13] Z. Altun, S. L. Carter, and H. P. Kelly, Phys. Rev. A **27**, 1943 (1983).
[14] P. Scott, A. E. Kingston, and A. Hibbert, J. Phys. B **16**, 3945 (1983).
[15] C. H. Greene and L. Kim, Phys. Rev. A **36**, 2706 (1987).
[16] T. Brage and C. Froese Fischer (unpublished).
[17] T. Brage, C. Froese Fischer, and G. Miecznik, J. Phys. B **25**, 5289 (1992).
[18] W. E. Baylis, J. Phys. B **1**, L583 (1977).
[19] A. Hibbert, Phys. Scr. **39**, 574 (1989).
[20] W. R. Johnson, D. Kolb, and K.-N. Huang, At. Data Nucl. Data Tables **28**, 333 (1983).
[21] P. M. Prenter, *Splines and Variational Methods* (Wiley, New York, 1975).
[22] C. de Boor, *A Practical Guide to Splines* (Springer-Verlag, New York, 1985).
[23] C. A. J. Fletcher, *Computational Galerkin Methods* (Springer-Verlag, New York, 1984).
[24] M. Landtman, C. Laughlin, Y.-T. Shen, and J. E. Hansen, J. Phys. B **26**, 1081 (1993).
[25] B. S. Garbow, J. M. Boyle, J. J. Dogarra, and C. B. Moler, *Matrix Eigensystem Routines—EISPACK Guide Extension* (Springer-Verlag, Berlin, 1977).
[26] R. Glass and A. Hibbert, Comput. Phys. Commun. **16**, 19 (1978).
[27] A. Hibbert, R. Glass, and C. Froese Fischer, Comput. Phys. Commun. **64**, 455 (1991).
[28] Q. Li, T. Lucatorto, T. Brage, and C. Froese Fischer (unpublished).
[29] J. Sugar and C. Corliss, J. Phys. Chem. Ref. Data **8**, 865 (1979).